Contents lists available at ScienceDirect

Remote Sensing of Environment

journal homepage: www.elsevier.com

Burn severity influence on post-fire vegetation cover resilience from Landsat MESMA fraction images time series in Mediterranean forest ecosystems

Alfonso Fernandez-Manso,[a] Carmen Quintano,[b,*] Dar A. Roberts [c]

[a] *Agrarian Science and Engineering Department, University of León, Av. Astorga s/n, 24400 Ponferrada, Spain*
[b] *Electronic Technology Department, University of Valladolid, Sustainable Forest Management Research Institute, University of Valladolid-Spanish National Institute for Agricultural and Food Research and Technology, C/Francisco Mendizábal, s/n, 47014 Valladolid, Spain*
[c] *Department of Geography, University of California, Santa Barbara, CA 93106, United States*

ARTICLE INFO

Article history:
Received 12 January 2016
Received in revised form 6 June 2016
Accepted 17 June 2016
Available online xxx

Keywords:
MESMA
SMA
Post-fire
Resilience
Vegetation cover recovery
Landsat
Mediterranean ecosystem
Pinus pinaster Ait.
Seeders
VRI

ABSTRACT

Mediterranean ecosystems are adapted to recurrent forest fires by having regeneration mechanisms that overcome the immediate effects of fire. However, the increasing frequency of fires in most European Mediterranean countries is challenging the natural regrowth capability of these ecosystems. In this context, monitoring post-fire vegetation recovery is a priority for forest management and soil erosion control. In this work, a 13-year series (1999–2011) of Landsat 5 Thematic Mapper (TM)/Landsat 7 Enhanced Thematic Mapper (ETM +) data was used to model post-fire vegetation recovery as a function of burn severity and to quantify post-fire resilience as a measure of vegetation cover regrowth. We evaluated a large forest fire located in Spain that burned approximately 30 km^2 of *Pinus pinaster* Ait. in August 1998. 88 field plots of four burn severity levels (unburned, low, moderate and high) were measured in the field a year after the fire. As a variable representative of vegetation, we chose the shade normalized green vegetation fraction image (SGV) obtained by applying Multiple Endmember Spectral Mixture Analysis (MESMA) to the original Landsat TM/ETM + images. The SGV values were extracted for the 88 field plots and, after performing a one-way analysis of variance (ANOVA), a Fisher's Least Significant Difference (LSD) test allowed us to estimate resilience of vegetation cover as the number of post-fire years exhibiting a statistically significant difference between burned and unburned areas. Next, SGV values were referenced to unburned control plots values and the vegetation recovery index (VRI) was defined. The evolution in time curve of VRI for low, moderate and highly fire affected vegetation was fit using trend models (specifically, an exponential trend for VRI in high and moderate burn severity levels; a linear trend for low burn severity level, Root Mean Square Error, RMSE = 0.18, 0.13, and 0.09, respectively). We observed that vegetation cover affected by low severity fire recovered to its original state after 7 years, and vegetation cover affected by moderate severity recovered after 13 years. Vegetation affected by high severity fire was estimated to recover after 20 years. We conclude that VRI time series based on multitemporal MESMA fractions from Landsat data can be considered a valuable indicator of the post-fire vegetation cover recovery. Its temporal evolution represented post-fire vegetation cover regrowth adequately and facilitated the estimate of vegetation cover resilience in Mediterranean forests.

1. Introduction

Mediterranean forest ecosystems are subjected to recurring fires, being their most significant disturbance (White et al., 1997). Accurate post-fire vegetation regeneration monitoring is a crucial conditioning factor for post-fire land management (Ruíz-Gallardo et al., 2004). As burned areas often have limited accessibility and cover large areas, satellite remote sensing and geographic information systems are considered essential for gathering and analyzing spatially explicit information, enabling the assessment of forest recovery after fire (Chuvieco, 2009; Gitas et al., 2012). With nearly 40 years of continuous observation, free Landsat imagery has become the most widely used information source to monitor vegetation dynamics (Bolton et al., 2015). Its spectral and spatial resolutions have demonstrated significant utility and the existence of a large number of images acquired over a single region have allowed for Landsat based time series analysis approaches. Since vegetation indices (or more generally spectral indices) from satellite imagery have been commonly used to monitor, analyze and map temporal and spatial dynamics of post-fire environments (Chu and Guo, 2014), spectral index time series analysis has been a multitemporal procedure particularly useful to monitor post-fire vegetation (Bastos et al., 2011; Chen et al., 2014; Dubovyk et al., 2015; Lanorte et al., 2014; Riaño et al., 2002; van Leeuwen et al., 2010).

Most of the studies related post-fire vegetation recovery are based on Normalized Difference Vegetation Index (NDVI) (Bastos et al., 2011; Ireland and Petropoulos, 2015; Petropoulos et al., 2014; Sever et al., 2012; Vicente-Serrano et al., 2011). There are, however, some examples based on other vegetation indexes as Enhanced Vegetation Index (EVI) (Abdul-Malak et al., 2015) or on the European Remote-Sensing (ERS) (C-band VV) backscatter coefficient (Polychronaki et al., 2014). However, post-fire environments are typically composed of vegetation and substrate. Thus, analysis of post-fire vegetation

* Corresponding author.

http://dx.doi.org/10.1016/j.rse.2016.06.015
0034-4257/

cover recovery using moderate spatial resolution sensors such as Landsat constitutes a sub-pixel mixing question (Veraverbeke et al., 2012). Though different sub-pixel image analysis techniques exist, linear Spectral Mixture Analysis (SMA) is the most often utilized (Quintano et al., 2012). This technique deals with mixed pixels by effectively defining independent endmembers that are supposed to represent the most important terrain attributes. SMA quantifies the sub-pixel fractional cover of each defined endmember. Compared to conventional spectral indices SMA is capable of detecting lower cover fractions and reduces the influence of background effects of soil color or moisture (Elmore et al., 2000). Additionally, fraction images from SMA are easier to interpret than spectral indices as they have a physical meaning (Adams et al., 1995). In terms of post-fire impacts, SMA has been used to analyze post-fire vegetation recovery in several studies (rather fewer than vegetation indices). Notable examples include papers by Riaño et al. (2002); Röder et al. (2008); Sankey et al. (2008); Smith et al. (2007); Souza et al. (2003); Twele (2004), Vereverbeke et al. (2012b) and Vila and Barbosa (2010). Multiple Endmember Spectral Mixture Analysis (MESMA), a modification of SMA, enables the use of multiple endmembers within a scene, making it possible to test different combinations of endmembers for each pixel in the image (Roberts et al., 1998). Though SMA fraction images have shown satisfactory results in post-fire vegetation studies, we are not aware of any examples that use MESMA to monitor post-fire vegetation cover recovery. For that reason, and hypothesizing that MESMA fraction images model each image pixel more accurately than SMA fraction images, our work proposes a MESMA-based method to monitor post-fire vegetation cover dynamics. If SMA fraction images have been used successfully to study post-fire vegetation cover recovery, MESMA fraction images should lead to more accurate results.

The capacity of an ecosystem to recuperate to its pre-disturbance (pre-fire) situation is quantified by its resilience. According to Díaz-Delgado et al. (2002) we measured resilience with reference to above-ground biomass. Instead of a qualitative evaluation of fire damage, resilience enables us to quantitatively estimate the economic losses attributable to the loss of access to some natural resources like timber, mushroom gathering or hunting as it measures the period of time during which the resources are not available (Rodrigues et al., 2014; Román et al., 2013). According to Sá-Torres (2013), post-fire resilience can be linked to biodiversity (e.g. Kazanis and Arianoutsou, 2004; Moreira et al., 2011; Pausas et al., 2008), vegetation structure (Keeley, 1986; Lee et al., 2009), or ecosystem function (e.g. Silva et al., 2011). Nevertheless, among the extrinsic factors that can modify the potential of an ecosystem to recover (resilience), burn severity understood as a measure of fire damage on vegetation cover is one of the most important (Bastos et al., 2011; Covington and Sackett, 1992; Neary et al., 1999; Röder et al., 2008; Smithwick et al., 2005).

Given the importance of burn severity to influence post-fire vegetation recovery, we organized our research in to three different burn severity scenarios (low, moderate and high burn severity level). Our study focuses on the potential of the combination of MESMA fraction images and time series analysis for monitoring and modeling post-fire vegetation cover recovery. As far as we know, this is the first post-fire resilience study that is based on MESMA fraction images time series. The main objective of the work was to quantify post-fire resilience for each burn severity level as a measure of vegetation cover recovery. To address it, we designed a research approach that tested the following hypothesis in Spain, in a forested area mainly covered by *P. pinaster* Ait. (a seeder), following a large forest fire that occurred in 1998: H1) The post-fire temporal evolution of MESMA green vegetation fraction images corresponds with the post-fire temporal evolution of the vegetation existent in study area; H2) The temporal evolution of the vegetation recovery index (VRI), defined on the basis of MESMA green vegetation fraction values extracted from field plots and referred to the unburned level, is also consistent with the post-fire temporal evolution of the vegetation cover; and H3) Trend modeling of VRI time series for each burn severity level enables us for making predictions about the post-fire resilience of the vegetation cover affected by each burn severity level.

2. Study area and dataset

2.1. Study area

'Tabuyo del Monte', our study area, is situated in the Sierra del Teleno, in Northern Spain (Fig. 1). Sierra del Teleno is a small series of mountains with an approximate altitude of 1100 m and an average slope of 10°. The climate is Mediterranean. The average annual rainfall ranges between 650 and 900 mm and there are 2–3 months of summer drought. This forest ecosystem has been frequently affected by fires, mainly due to dry spring-summer storms that predominantly damaged small areas. We studied the burn severity evolution on a large fire, which burned around 30 km^2 during 4 days, between 13 and 17, September 1998. Specifically, from official post-fire data: 63% of burned area had a high severity level, 21% a moderate severity level and 16% a low severity level. Subsequently, another fire burned 117.75 km^2 between 19 and 21 September, 2012. This fire overlapped 60% of the area burned by the 1998 fire (see Fig. 1).

According to the Spanish Forestry Map, the burned area was covered by *Pinus pinaster* Ait. (76%), *Quercus ilex* L. (7%), *Quercus pyrenaica* Willd (5%), *Pinus sylvestris* L. (2%), and shrubs (10%) (*Calluna vulgaris* (L.) Hull, *Chamaespartium tridentatum* (L.) P.E. Gibbs, *Erica australis* L., *Halimium alyssoides* Lam and *Genista florida* L.). Before the 1998 fire, 60–85 year old *P. pinaster* stands dominated the vegetation, with 95% cover, and a density of 500–900 trees/ha (Calvo et al., 2008).

P. pinaster is a seeder. Similar to other Mediterranean *Pinus* species, such as *Pinus halepensis* Mill., *P. pinaster* reacts to fire by a rapid seed dispersal that starts at the beginning of fire and continues for a few months after the fire is extinguished (Herranz et al., 1997; Thanos et al., 1996). For *P. pinaster*, established temperature ranges cause post-fire germination seeds; specifically, as expressed by Herrero et al. (2007), the temperature range between 70 and 110 °C germinates *P. pinaster* seeds, regardless of exposure time. When the time of exposure is high a successful regeneration will be possible up to 130 °C. Exceptionally, post-fire germination seeds will be possible up to 190 °C for short time of exposure (rapid fires). However, as suggested by Calvo et al. (2008), the *P. pinaster* population in the study area has some anatomical and physiological characteristics that differ from any other Spanish natural population of *P. pinaster*, potentially caused by frequent recurrence of fires in the area. Among these adaptations, the most noticeable may be high production of serotinous cones (that protect the seeds), thicker bark, resistance to lower temperatures, and a significantly earlier flowering age (Tapias et al., 2004).

2.2. Ground measured data

A year after the fire (September 1999) burn severity level was measured on 88 100-m diameter field plots of *P. pinaster* (Fernández-Manso et al., 2009). Large areas with similar fire severity levels and low slope gradients were pre-selected using post-fire ortho-photographs. Inside these areas, the field plots were randomly lo-

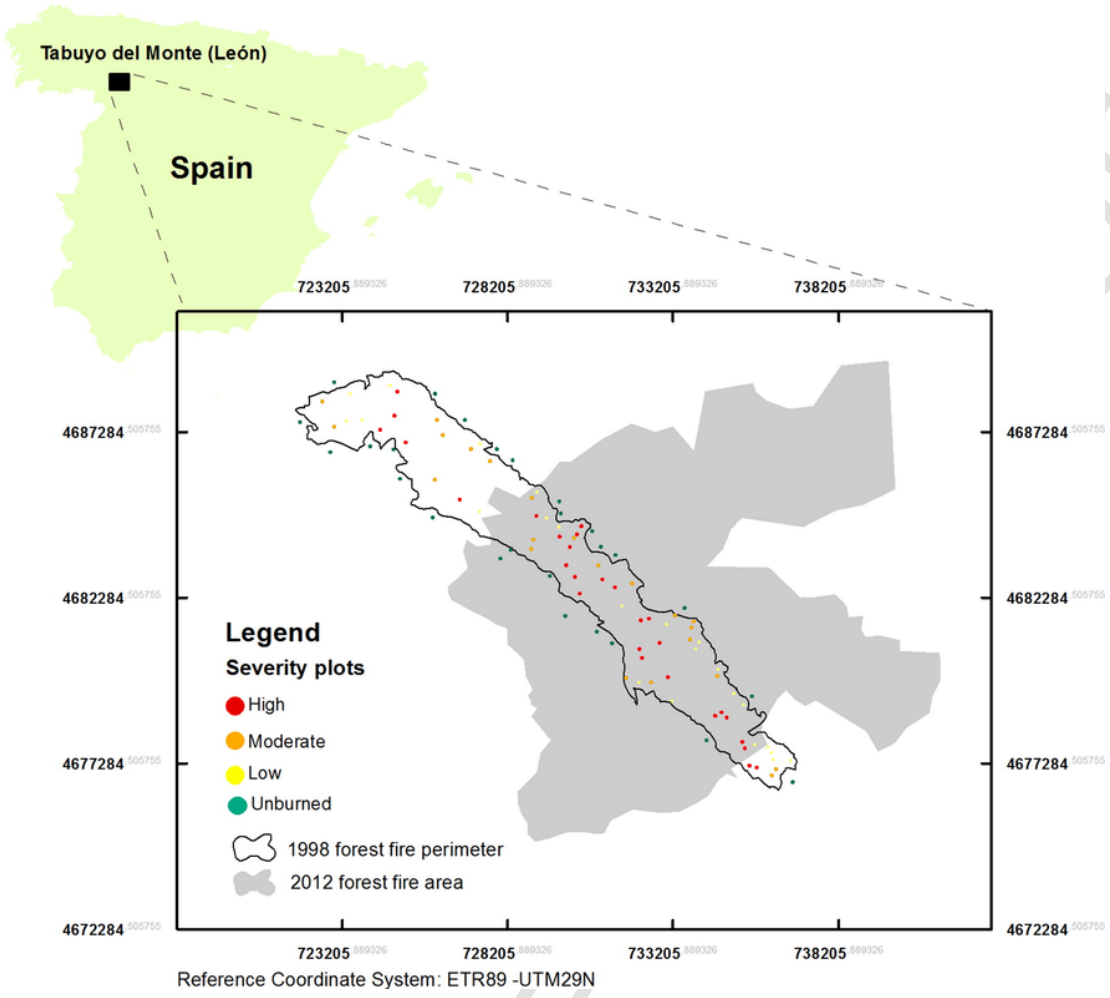

Fig. 1. Location of study area, 1998 fire perimeter and field plots classified by burn severity level. Area affected by the 2012 forest fire is also represented.

cated. Unburned areas were chosen next to burned ones, resulting in similar topography, surficial geology, and vegetation to the burned areas as recommended by Díaz-Delgado et al. (2002). Despite the one-year time lag, we found a quantity of scorched leaves (on branches and the ground) and of char on the tree trunks adequate to evaluate the burn severity level qualitatively. The assessment performed within the first growth season after fire (EA, extended assessment) may yield a characterization of actual fire effects more complete that the provided by a initial assessment (IA), since EA includes first-order effects as delayed mortality of vegetation and survivorship (Key and Benson, 2006).

We defined four burn severity levels in accordance with the degree of scorching vegetation: unburned, low, moderate and high (see Fernández-Manso et al., 2009 for more details). Specifically, a low burn severity level was assigned to areas with burned shrubs to 2 m and no or partially scorched canopy; a moderate burn severity level was assigned to areas with incinerated shrubs and scorched canopy, and high burn severity was assigned to areas with incinerated shrubs and completely burned and apparently dead canopy, even though some plants may still be able to sprout. Similar criteria were used by previous studies (e.g. Jakubauskas et al., 1990; Patterson and Yool, 1998; Rogan and Yool, 2001) since a standard method to field measure burn severity, such as the Composite Burn Index, was not commonly accepted until approximately 2006 (Key and Benson, 2006). Each plot was assigned to one of the four defined burn severity levels considering the majority burn severity class observed in each plot. We measured 18 low-burn severity plots, 19 moderate-burn severity plots, 27 high-burn severity plots and 24 unburned plots, where *Pinus pinaster* was the dominant specie in all of them.

2.3. Remote sensed data

A time series of Landsat images (1999–2011) was downloaded from the US Geological Survey (USGS) Global Visualization Viewer (GLOVIS): 12 Landsat 7 ETM + images and 2 Landsat 5 TM. We selected images by choosing a similar date of acquisition and minimizing cloud cover, and illumination and phenological changes. The central date of images was day 212 (31 July), with a mean solar zenith of 32° and a mean solar azimuth of 134° (Table 1). Fortunately, the Scan Line Corrector failure did not affect our field plots (with the exception of two in 2006, high burn severity and unburned, and one in 2008, moderate burn severity). However, we had to limit the time series to the period 1999–2011 because the 2012 mega-fire burned approximately 60% of the area burned by the 1998 fire and 80% of our field plots (see Fig. 1).

Table 1
Summary of Landsat images used.

Date (dd/mm/yyyy)	Date (Julian day)	Satellite/Sensor	Solar zenith (°)	Solar azimuth (°)
01/07/1999	182	L7/ETM +	26	128
04/08/2000	217	L7/ETM +	32	134
20/06/2001	171	L7/ETM +	26	127
25/07/2002	206	L7/ETM +	30	130
05/08/2003	217	L5/TM	34	129
16/09/2004	260	L7/ETM +	44	148
01/07/2005	182	L7/ETM +	27	127
21/08/2006	233	L7/ETM +	36	139
31/07/2007	212	L5/TM	30	134
09/07/2008	191	L7/ETM +	28	127
29/07/2009	209	L7/ETM +	30	132
31/07/2010	212	L7/ETM +	31	133
27/09/2011	263	L7/ETM +	46	151
Mean values	212		32	134

2.4. Ancillary data

A post-fire 0.7 m color aerial photograph from Autonomous Government of Castilla and León (JCyL) collected immediately after the fire, helped us locate homogeneous areas to situate the field plots and to define the endmember spectra. In addition, we also used three 0.7 m digital ortho-photographs acquired in 1999, 2006 and 2011, respectively. Ortho-photos were supplied by the Spanish National Center of Geographic Information (CNIG; http://www.cnig.es/) through the Spanish Aerial Ortho-photography National Planning (PNOA) agency. A USGS supplied ASTER Global Digital Elevation Model Version 2 (GDEM V2) was used to topographically normalize the Landsat images.

Additionally, we utilized an Airborne Visible/Infrared Imaging Spectrometer (AVIRIS) image of Santa Barbara, California to obtain ash spectra. The image was acquired on 26 August 2009, 3 months after the May 2009 Jesusita fire. Modtran radiative transfer code and a ground reference target allowed to correct the image atmospherically and converted it to reflectance (see Herold et al., 2004; Roberts et al., 2012).

3. Methods

The methodology comprised three main steps: 1) pre-processing of Landsat 5 TM/Landsat 7 ETM + images, including image subsetting, topographic normalization, atmospheric correction, and radiometric normalization; 2) the MESMA procedure, that included creation of a spectral library with the most appropriate endmembers, and spectral unmixing of Landsat pre-processed images; and 3) statistical analysis to model the post-fire VRI temporal evolution (1999–2011) for each burn severity level (Fig. 2). Similar to Díaz-Delgado et al. (2002) in their NDVI based study about post-fire resilience of Mediterranean plants, we assumed that the green vegetation (GV) fraction images (step 2) are a reasonable representation of green vegetation cover, with the following conditions: 1) though GV fraction images do not provide us a highly detailed analysis, we can observe in them general structures and trends in relative vegetation amount; 2) if the GV fraction image is saturated and does not show the high levels of green vegetation that are actually present, the error level will be higher; and 3) we will transform the original GV fraction values to maximize the information related to the ground components of interest. The VIPER Tools 1.5 software tool (www.vipertools.org) (Roberts et al., 2007), an IDL-based ENVI (Exelis Visual Information Solutions) extension, was used to perform the MESMA procedure including the spectral library building, optimal endmember selection and the unmixing processes.

The statistical analysis (step 3) enabled us to test the initially proposed hypotheses. Regarding H1, one-way analysis of variance (ANOVA) of 2006 and 2011 shade normalized green vegetation fraction values from the field plots grouped by burn severity levels helped us to identify the significance of different burn severity levels. If there were no significant differences between a burn severity level and the unburned class, we would assume that vegetation cover affected by such burn severity level had returned to initial conditions (resilience cycle). The potential recovery vegetated cover in field

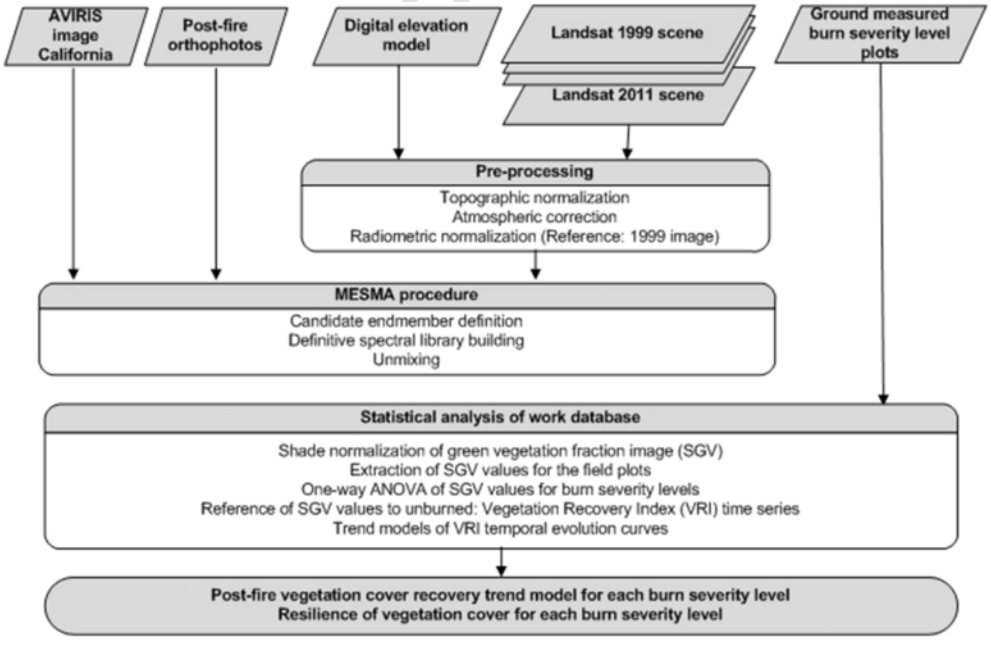

Fig. 2. Flowchart of methodology.

plots was checked visually from 2006 and 2011 ortho-photographs, being a qualitative validation. With respect to H2, the post-fire temporal evolution of VRI for each burn severity level was depicted and visually compared to the previous mentioned ANOVA results (paying special attention to years 2006 and 2011). Finally, the three VRI time series were trend modeled, what correspond to *H*3.

3.1. Preprocessing of the Landsat images

All Landsat scenes (path/row 203/31) were downloaded from the USGS with an L1G level of processing (radiometric and geometric corrected, and geo-referenced to the Universal Transverse Mercator (UTM) map projection). Next, we co-registered the images to the digital orthophotos supplied by CNIG and JCyL. A mis-registation error below 0.25 of a Landsat pixel was found between post-fire false-color orthophotos and the Landsat images. After co-registration, we subset the images to the selected forest fire. The C-correct approach (Teillet et al., 1982) and the GDEM V2 DEM from USGS were used to topographically normalize the subset images using the R software environment. Finally, all images were scaled to apparent surface reflectance. We used the procedure suggested by Chander et al. (2009) to convert the original digital numbers to radiance values (L_λ), and the image-based cosine of the solar transmittance (COST) method (Chavez, 1996), to convert radiance to surface reflectance (ρ). The formulae described in Song et al. (2001) assuming 1% surface reflectance for dark objects (Chavez, 1989, 1996) allowed us to calculate the path radiance (L_p) values. We estimated the optical thickness for Rayleigh scattering (ρ_r) following the equation specified in Kaufman (1989).

SMA requires radiometric similarity among multi-temporal input images because data quality and image radiometric normalization affects the results of change detection procedures (He et al., 2011). For this reason, the reflectance images were normalized to a reference image to minimize the impact of sun-sensor-view angle differences. To perform this normalization we used the iteratively re-weighted multivariate alteration detection (IRMAD) algorithm (Canty and Nielsen, 2008). The IRMAD normalizes images such that they appear to have been obtained by the same sensor subject to atmospheric and illumination conditions almost identical to those of the reference image (Yang and Lo, 2000). The first image of the time series (1999) was used as reference based on its proximity to the forest fire date. In this way, definition of ash endmembers would be expected to be more accurate.

3.2. MESMA procedure

MESMA is a linear SMA where different mixing models are examined in each pixel to minimize model error (Roberts et al., 1998). Linear SMA represents each pixel as a weighted linear combination of a limited number of endmembers describing the whole scene, with the endmember fractions acting as the weight and spectral departures from the model expressed as a residual (Eq. (1)):

$$x = Mf + e \quad (1)$$

where, x is a measured Landsat spectrum modeled as a 6-dimensional reflectance vector consisting of up to four endmembers (M), multiplied by endmember fraction f; and e is a 6-dimensional error vector representing the residual error. Least-squares solution (Shimabukuro and Smith, 1991) or singular value decomposition (Boardman, 1990) are methods often used for solving Eq. (1) because to its simplicity and ease of implementation. The root-mean-square error (RMSE) is utilized to measure model error (Roberts et al., 1998).

MESMA allows each pixel to be unmixed by a different model (or set of endmembers). In this way, the number of materials in which a scene can be unmixed is not restricted to the number of endmembers used. The model selected to unmix each pixel is the one that minimizes the RMSE. As happens with linear SMA, endmember choice is a key stage to the successful result of the MESMA procedure. The unmixing accuracy is determined by the endmember selection (Tompkins et al., 1997; Li et al., 2005;). Too many endmembers may overfit the data producing an unstable solution. By contrast, if the number of endmembers is too low, large residual errors will be obtained, as the fraction of unmodeled features will be distributed among the fractions of the selected endmembers (Li et al., 2005). Fraction accuracy decreases when inversion of Eq. (1) becomes unstable due to the non-orthogonality of the endmembers matrix. The matrix becomes non-orthogonal when collinearity or multi-collinearity appears as a consequence of a high correlation between endmembers (van der Meer and Jia, 2012). Linear independency, spatial generality and spectral representativity are characteristics of an ideal set of endmembers (Maselli, 1998).

Unlike SMA, MESMA needs a large library of endmembers (obtained from the image field, and/or laboratory) representative of each ground component (Okin et al., 2001). The endmember spectra must have recognizable characteristics in the scene and must be meaningful for the user, since they are regarded as abstractions of physical objects that have the same or similar properties (Quintano et al., 2012). There are two broad alternatives to select the adequate endmember: reference endmembers from spectral libraries or image endmembers from the image itself. Image endmembers have two advantages: they were measured at the same scale as the image data and they are relatively easy to obtain. We formed our spectral library using mainly image endmembers (see Fig. 3). Following previous studies (Hostert et al., 2003; Riaño et al., 2002; Röder et al., 2008; Silván-Cárdenas and Wang, 2014), all time series images were unmixed using the same endmember spectra set to avoid variability in the interpretation among all dates. The endmembers spectra were obtained from the first post-fire image of time series because vegetation regeneration hampered the definition of ash image endmembers in the last Landsat images. Moreover, as our first post-fire image was acquired a year after the fire, and most ash had disappeared due to erosion by wind and rain, we complemented the image endmembers with ash spectra from the post-fire AVIRIS image of California area, previous resampling to Landsat wavelengths.

Similar to Dudley et al. (2015), we defined potential endmembers using a set of georeferenced polygons. We searched for uniform polygons of just one class within the post-fire orthophotograph. The polygons covered all three levels of burn severity (38 polygons, 750 pixels), over different kinds of soil (16 polygons, 225 pixels), and over the different types of unburned vegetation (green and non-photosynthetic) (42 polygons, 825 pixels), and were stored in a shape file.

A key step of mixture modeling is to identify the endmembers that best characterize a particular ground component and are least likely to be modeled by another component (Tompkins et al., 1997). Since a spectral library can incorporate hundreds of spectra for each ground component it is necessary to take into account not only the spectral diversity of the library but also the computational efficiency (Dennison and Roberts, 2003b; Dennison et al., 2004). To form our definitive spectral library, three techniques were used to choose the most suitable endmembers from a computationally high number of candidate endmembers: Count-based Endmember Selection (CoB) (Roberts et al., 2003), Endmember Average RMSE (root mean

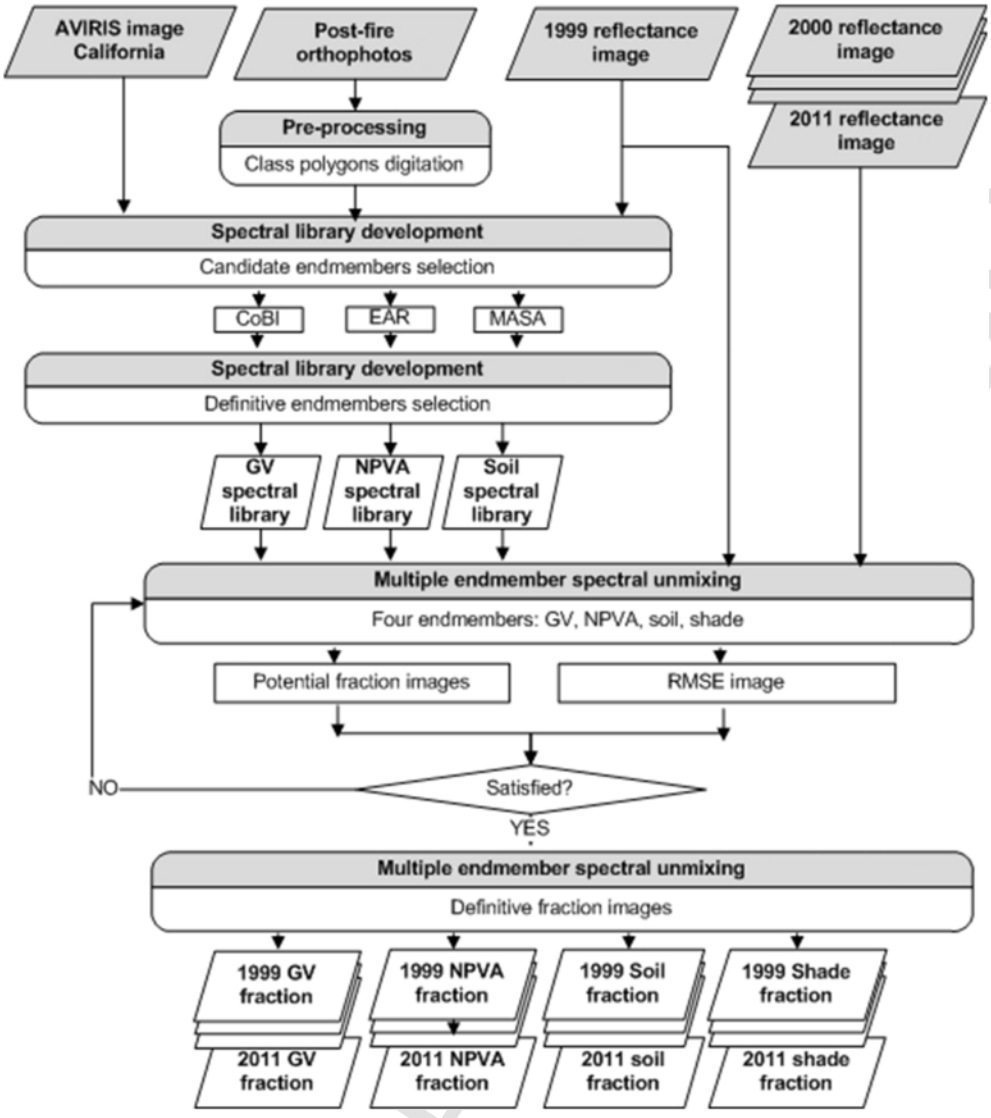

Fig. 3. Flowchart of MESMA procedure.

squared error) (EAR) (Dennison and Roberts, 2003a), and Minimum Average Spectral Angle (MASA) (Dennison et al., 2004). Using CoB we selected the endmembers that model the greatest number of endmembers within their class. When EAR was considered, we chose endmembers that yield the lowest RMSE within a class. Finally, we chose the endmembers with the lowest average spectral angle when MASA was taken into account. VIPER Tools open-software incorporates all of them. In addition, as recommended by Roberts et al. (2007) we considered the typical spectral shape of the selected spectra and our knowledge of the study area.

Following Quintano et al. (2013), who mapped burn severity from Landsat images using MESMA, we grouped the endmembers into the following three spectral libraries: green vegetation (GV); non photosynthetic vegetation and ash (NPVA); and soil. Therefore, using MESMA the Landsat images were unmixed into four endmembers: GV, NPVA, soil and shade. For each pixel, the performance of all models was assessed by considering fraction images, the shade fraction image and RMSE. Similar to Powell et al. (2007); Quintano et al. (2013); Roberts et al. (2003), and Roberts et al. (2012), we made use of the following selection criteria: − 0.05 and 1.05, as the minimum and maximum permissible fraction values; 0.8 as maximum permissible shade fraction value, and 0.025 as maximum permissible RMSE. If several models satisfied these conditions, the model that generated the lowest RMSE was chosen. We established threshold of 90% as the minimum number of classified pixels for a viable model; meaning that the MESMA fraction images were only definitely accepted if the number of classified pixels of each Landsat image was above 90%. If this condition was not fulfilled we unmixed all of the images again while varying the type and/or number of spectra comprised in each spectral library. Fig. 3 displays a flowchart of the MESMA procedure.

3.3. Statistical analysis of work databases

GV MESMA fraction images were shade normalized using the VIPER Tools 1.5 software tool, previously used to obtain the MESMA fraction images. Shade normalization removes the shade fraction, redistributing this fraction proportionally among all other non-shade endmembers (Roberts et al., 2007; Rogan and Franklin, 2001). Values from shade normalized GV fraction images (SGV) were extracted for the 88 field plots to complete the work database to be statistically analyzed.

First, we performed one-way (ANOVA) of SGV values grouped by burn severity level. The Fisher's least significant difference (LSD) test was accomplished to identify the sample means that were significantly different from other ones. Specifically to validate H1, the LSD test results of years 2006 and 2011 were evaluated. From then we verified whether there were significant differences between burn severity levels and the unburned class. If there were no significant differences, we assumed that the vegetation cover affected by such burn severity level regrows to its pre-fire situation (resilience cycle). This supposition was validated analyzing the field plots visually over the 2006 and 2011 post-fire ortho-photographs. In addition, ANOVA helped us to estimate the resilience of vegetation for each burn severity level, since we could identify the year where there was no significant differences between burn severity levels and the unburned class.

Second, to model post-fire vegetation recovery and establish the vegetation cover resilience, the post-fire condition of vegetation should be compared to its pre-fire situation. Since the first cloud-free pre-fire image we found in the UGSG-GLOVIS system was acquired on September 1990, 9 years before our first time series image, we based our study on the unburned control plot approach (Díaz-Delgado and Pons, 2001), that considers the unburned vegetation in each image as the pre-fire reference, reducing the influence of phenologic changes. Thus, we defined VRI for each burn severity level and year (Eq. (2)) as the average SGV value for such burn severity level and year referenced to the unburned control plots. VRI would represent the increase of forest canopy cover for each burn severity level. When VRI reaches the zero level we could think that the "increase of forest canopy cover" has ended because the vegetation cover has reached its initial or pre-fire values. Moreover, VRI made easier the visualization of the vegetation cover regeneration curve for the three burn severity levels, as the same reference is considered as origin (unburned class, zero value). Visual analysis of VRI temporal curves simplified the understanding and selection of the more suitable trend model for each VRI time series.

$$VRI_j = \frac{\overline{SGV_j} - \overline{SGV_u}}{\overline{SGV_j} + \overline{SGV_u}} \quad (2)$$

where: 'j' represents a burn severity level (low, moderate, high); $\overline{SGV}_j$, the mean SGV value of field plots of 'j' burn severity for the considered year; and $\overline{SGV}_u$, the average SGV value of unburned field plots for the same year. In this way, we computed three VRI values for each Landsat image: one for low burn severity level (VRI_l), another for moderate (VRI_m) and another one for high burn severity level (VRI_h). Thus, three VRI time series were built. For each time series, if VRI equals zero, the vegetation has reached its original state, and the x-axis value for which VRI = 0 will show the resilience time of vegetation cover in years after fire. If the temporal evolution of the three VRI time series is consonant with the previous mentioned LSD test results, we could consider H2 as validated.

Finally, as a preliminary step to trend modeling the three VRI time series, their potential randomness was checked. We used three statistical tests because each of them detects a type of deviations from random response. The time series will not be considered completely random when any test is not passed. The three tests were: 1) to count how many times the sequence was above or below the median, 2) to count how many times the sequence rose or fell, and 3) to considerer the sum of squares of the first 24 autocorrelation coefficients (Statpoint Technologies, 2012).

After verifying that the VRI time series were not random, we identified the model that better suited each time series. Three trend models were considered as candidates: mean, linear trend, and exponential trend. All three types of recovery models were fit to the data by least squares, using time as the independent variable (Eqs. (3)–(5)).

$$\text{Mean}: F_t(k) = \overline{Y}_t \quad (3)$$

$$\text{Linear trend}: F_t(k) = a_0 + a_1(t+k) \quad (4)$$

$$\text{Exponential trend}: F_t(k) = e^{(a_0 = a_1(t=k))} \quad (5)$$

where: t, t = 1, 2, … n, is the time (years) after fire event; n is the simple size used to fit the model; $F_t(k)$ is the forecast for time t + k made at time t; Y_t is the observed value at time t; a_0, a_1, and a_2 are the coefficients of the regression models.

Selection of the best-fit trend model was made considering three values: RMSE, calculated by estimating the standard deviation of the one-ahead forecast errors; mean absolute percentage error (MAPE), calculated by estimating the average percentage one-ahead forecasting error and the Akaike information criterion (AIC), a function of the variance of the model residuals, penalized by the number of estimated parameters (Eqs. (6)–(8)).

$$RMSE = \sqrt{\frac{\sum_{i=1}^{m} e_{n+i}^2}{m}} \quad (6)$$

$$MAPE = 100\frac{\sum_{i=1}^{m}\left|\frac{e_{n+i}}{Y_{t+i}}\right|}{m} \quad (7)$$

$$AIC = 2\ln(RMSE) + \frac{2\cdot c}{n} \quad (8)$$

where: n is the simple size used to fit the model; m is the number of validation observations at the end of the time series, e_t is the one period ahead forecasting errors calculated from $e_t = Y_t - F_{t-1}(1)$; and c is the number of estimated coefficients in the fitted model.

Small values of RMSE and MAPE are desirable. As a rule, the model that minimizes first the mean squared error than the number of coefficients (compared to the quantity of data available) is the model that will be chosen. Once a model has been selected, we validated it by analyzing its residuals. Several tests were applied to the forecast errors to verify whether the model had accounted for all of the structure in the data: RUNS, a test based on the number of runs up and down; RUNM, a test based on the number of runs above and below the median; AUTO, a chi-squared test based on the first residual autocorrelations; MEAN, a t-test comparing the mean residuals in the first and second halves of the data; and VAR, an F-test comparing the variance of the residuals in the two halves (Statpoint Technologies, 2012).

4. Results

Fig. 4 shows some examples of the endmember spectra comprised in each spectral library. Table 2 shows the number of models used in the MESMA procedure and the percentage of pixels classified. Although we defined a minimum threshold of 90% in the number of classified pixels, using the definitive spectra libraries to perform the unmixing, the mean number of classified pixels was 95.6. The number of classified pixels is remarkably high considering that we unmixed 13 images using the same spectral libraries.

Fig. 5 shows the set of shade normalized fraction images from the 1999 Landsat 7 ETM + image. We can clearly see the burned area (dark pixels) from the SGV fraction image. The shade normalized NPVA fraction image displays the burned area and the un-irrigated lands. Finally, the shade normalized soil fraction image shows clearly soils, paths and small roads.

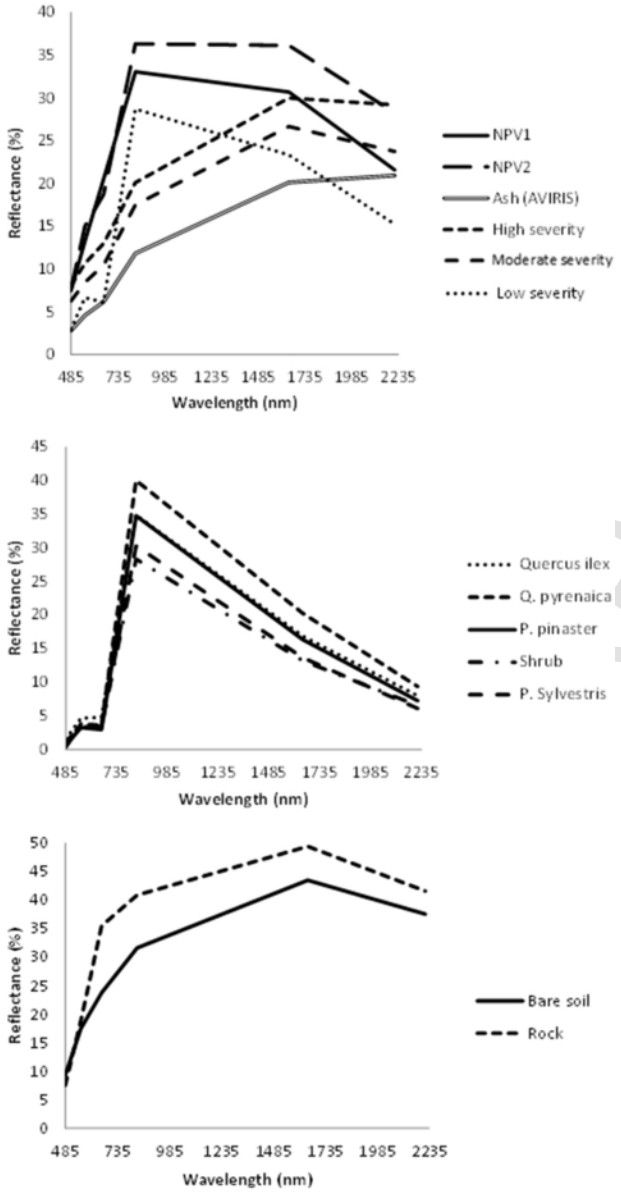

Fig. 4. Examples of endmembers signatures.

Table 2
MESMA procedure: spectral libraries, endmembers used and percentage of image classified pixels.

NPVA spectral library		GV spectral library		Soil spectral library	
Endmembers	Number	Endmembers	Number	Endmembers	Number
Ash	2	*Pinus pinaster*	2	Rock	1
High burn severity	2	*Quercus ilex*	1	Bare soil	1
Moderate burn severity	1	*Quercus pyrenaica*	1		
Low burn severity	1	*Pinus sylvestris*	1		
NPV 1	1	Shrubs 1	1		
NPV 2	1	Shrubs 2	1		

MESMA procedure							
Year	1999	2000	2001	2002	2003	2004	2005
Image classified (%)	96.9	96.62	96.35	95.32	96.68	94.51	94.16
# Models used	112	112	112	112	112	112	112

Year	2006	2007	2008	2009	2010	2011
Image classified (%)	93.79	96.69	95.07	94.67	95.27	97.69
# Models used	112	112	112	112	112	112

NPVA: no photosynthetic vegetation and ash; GV: green vegetation; NPV: no photosynthetic vegetation.

The evolution in time of the SGV fraction images is shown in Fig. 6. Left, we can observe the initial SGV fraction image (from 1999 Landsat 7 ETM + image). The SGV fraction image from the 2006 Landsat scene is shown in the center. Inside the fire perimeter it is possible observe some white areas (vegetated areas). Finally, the 2011 SGV fraction image is shown at the left corner. It is notable that most of the area inside the fire perimeter appears in white tones indicating a high green vegetation level.

Table 3 displays the results of the Fisher's LSD test for the SGV images and burn severity levels. The first year after fire (1999) the four SGV severity levels (unburned, low, moderate and high burn severity level) were found to be significantly different. In following years after fire, only 3 SGV levels were significantly different. The low burn severity class was grouped with the unburned class 7 years after the fire, meaning that there were no significant differences between these two levels. Thus, resilience of vegetation affected by low burn severity was found to be 7 years. Finally, there were only two SGV values that were significantly different in 2011 (high burn severity level and a mix of moderate, low and unburned), suggesting that resilience of vegetation affected by moderate burn severity level was 13 years.

From Table 3 it can be observed that the field plots affected by low burn severity in 2006 had no significant differences with unburned field plots. By 2011 moderate severity field plots were not significantly different than unburned field plots. Checking the post-fire evolution of the 18 low burn severity plots using the 2006 ortho-photograph, we verified that most of them were covered by green vegetation (specifically, we only found two field plot where we could not observe full regrowth). Concerning the 19 moderate burn severity plots, we confirmed using the 2011 ortho-photograph that all of the field plots except one showed full regrowth.

The Fig. 7 shows the evolution in time of the VRI values with the unburned reference as the x-axis (zero value). Again, we can see a rapid decrease in VRI for the three burn severity levels classes during the three first years after fire (meaning a high recovery of the vegetation cover). Following this period, the high and moderate burn severity affected vegetation remained almost constant until 11 years after the fire, when the vegetation experienced a relatively important increase again. In contrast, after the 3rd year following fire, the low

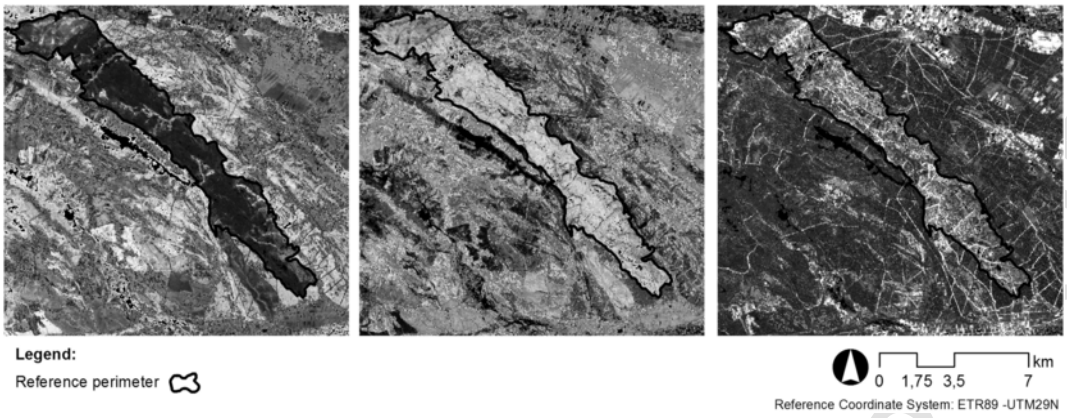

Fig. 5. MESMA shade normalized fraction images from the 1999 Landsat 7 ETM + image: left, shade normalized green vegetation fraction; center: shade normalized non-photosynthetic vegetation and ash fraction; right: shade normalized soil fraction.

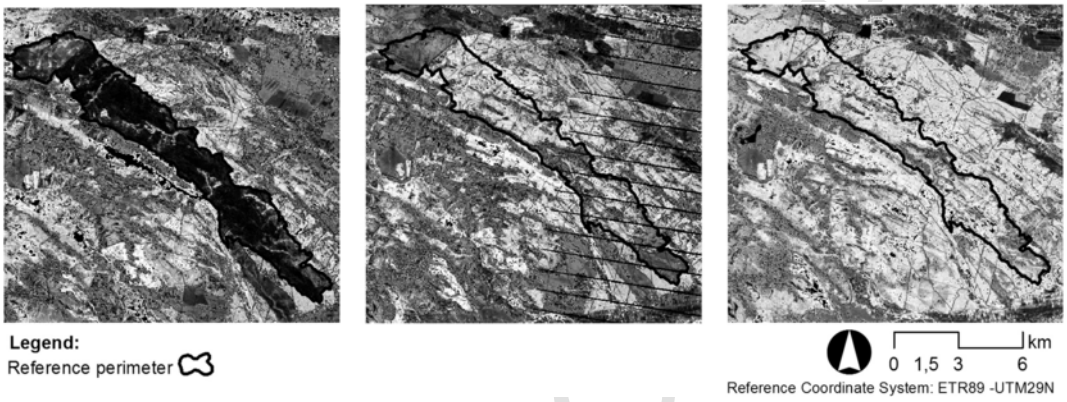

Fig. 6. Shade normalized green vegetation fraction images, 1999 (left), 2006 (center), and 2011 (right).

burn severity level class decreased slowly and reached the x-axis (unburned level) around the 7th year after fire. The moderate severity level almost declined to the unburned level (0.018) after 13 years (last year of time series). Vegetation affected by high burn severity remained at the 0.100 value by the end of the study period.

The three statistical test for randomness confirmed the three VRI time series could not be considered random. Table 4 shows the trend models that best fit the VRI evolution in time curves. The exponential trend model had the lowest RMSE and MAPE values and the highest AIC values for high and moderate fire affected vegetation. For the low burn severity class, however, a linear trend was selected. The exponential trend model was not considered because clearly it did not fit the VRI_l time series. From the analysis of Table 3 and Fig. 7 we can clearly conclude that vegetation cover affected by fire with low severity reached its initial state around 7 years after fire whereas vegetation cover affected by moderate burn severity needed 13 years. In both cases, the initial state of vegetation cover was reached during the period of time analyzed by the time series. For that reason, we only made predictions from the exponential trend model of VRI_h. A 7 year prediction (half of the period of time of time series) was considered. The exponential trend model of VRI_h forecasted a value of 0.058 by 2018 (with a lower limit of the confidence interval at 95% equals to 0.018 and an upper limit of 0.191). From this forecast we can conclude that vegetation affected with high severity level, would reach its initial state after 20 years.

5. Discussion

Spectral indices have been widely used to monitor post-fire vegetation regeneration (Bastos et al., 2011; Chen et al., 2011; Di Mauro et al., 2014; Goetz et al., 2006; Meng et al., 2015). However, spectral changes related to vegetation recovery can be observed in more than just two spectral bands. Fraction images, by contrast, did not have this shortcoming, and accurate estimates of vegetation abundance can be achieved when vegetation cover is low, i.e. the first years of regeneration after a forest fire (Tapias et al., 2004). Despite the lack of studies based on MESMA fraction images to monitor post-fire vegetation dynamics, SMA-based fraction images were successfully used. Among others, Smith et al. (2007) concluded that SMA fraction images were a marginally improved predictor of one-year post-fire conditions, compared to widely used spectral indices like dNBR. Sankey et al. (2008) confirmed the use of SMA fraction images to study the post-fie recovery of shrub canopy cover in 16 different fires in Idaho (USA). Twele (2004) affirmed that SGV was highly correlated with field measurements, enabling its interpretation as a physical variable. Our results agree with the findings of these studies extending the applicability of MESMA. In the above mentioned studies, linear SMA made use of just one set of endmembers to unmix to the whole image (typically a vegetation endmember, a soil endmember and a shade endmember). As we used a higher number of endmembers (specifically, 7 green vegetation and two non-photosynthetic vegetation endmembers; two types of soil endmembers and four endmembers of

Table 3
Fisher's least significant difference test for the SGV images and burn severity levels.

Burn severity level	Years after wildfire																							
	1 (1999)		2 (2000)		3 (2001)		4 (2002)		5 (2003)		6 (2004)		7 (2005)		8 (2006)		9 (2007)		10 (2008)		11 (2009)		12 (2010)		13 (2011)	
	⌠(SGV)	HG	⌠(SGV)	HG	⌠(SGV)	HG	⌠(SGV)	HG	⌠(SGV)	HG	⌠(SGV)	HG	⌠(SGV)	HG	⌠(SGV)	HG	⌠(SGV)	HG	⌠(SGV)	HG	⌠(SGV)	HG	⌠(SGV)	HG	⌠(SGV)	HG
High	0.0153	a	0.2714	a	0.4291	a	0.4291	a	0.4841	a	0.4749	a	0.4480	a	0.4786	a	0.4583	a	0.4538	a	0.4601	a	0.4997	a	0.5566	a
Moderate	0.0929	b	0.3216	a	0.4579	a	0.5279	b	0.5925	b	0.6030	b	0.5850	b	0.5954	b	0.6317	b	0.6121	b	0.5980	b	0.6218	b	0.6571	b
Low	0.2431	c	0.4663	b	0.5481	b	0.6081	c	0.6228	b	0.6368	b	0.6754	c	0.6563	c	0.6970	c	0.6780	c	0.7051	c	0.6740	c	0.7060	b
Unburned	0.6533	d	0.6897	c	0.6472	c	0.6472	c	0.7059	c	0.7099	c	0.6900	c	0.6969	c	0.6816	c	0.6793	c	0.7041	c	0.6735	c	0.6814	b
# Groups	4		3		3		3		3		3		3		3		3		3		3		3		2	
P-value	0.0000		0.0000		0.0000		0.0001		0.0000		0.0001		0.0000		0.0000		0.0000		0.0001		0.0001		0.0010		0.0010	

HG: homogeneous groups; ⌠(): mean value; SGV: shade normalized green vegetation fraction image.

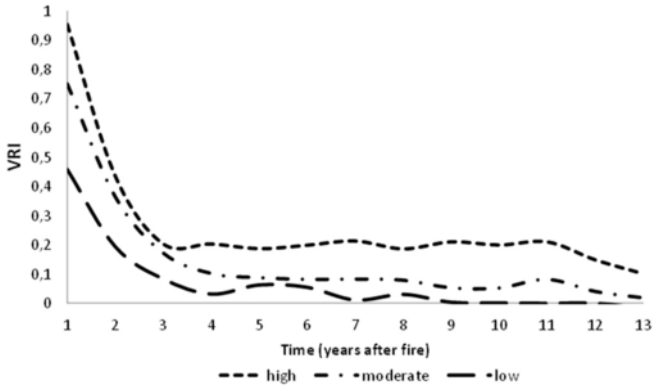

Fig. 7. Temporal evolution vegetation recovery indexes (VRI).

burned vegetation) the fraction images we obtained presumably were more accurate than the obtained by simple SMA.

The unburned control plot procedure, which is widely used in NDVI-based studies related to the post-fire vegetation recovery (Díaz-Delgado et al., 2002; Idris et al., 2005; Lhermitte et al., 2010, 2011; Li et al., 2008; van Leeuwen et al., 2010; Veraverbeke et al., 2011), has not to our knowledge been applied to fraction images. Our study validated its use with MESMA SGV fraction images. The unburned control plot procedure established an unburned reference to compute VRI for each burn severity level. As the evolution in time of these three VRI time series showed different vegetation cover recovery patterns, it was concluded that burn severity has a great impact on the capability of a system to recover to its initial conditions, as previous studies showed (Covington and Sackett, 1992; Maia et al., 2012; Neary et al., 1999; Röder et al., 2008; Smithwick et al., 2005).

Previous studies (Keeley et al., 2012; Twele, 2004) also revealed a strong correlation between pre-fire vegetation type and regeneration process. The vegetation cover regrowth patterns we found (Tables 3 and 4 and Fig. 7) agreed with the results of previous non-remote sensing-based studies also centered on *P. pinaster*. In our study area, Calvo et al. (2003, 2008, 2013) concluded that the dominant species, *P. pinaster*, had a predominantly high rate of natural regeneration. Mean seedling height showed a significant increase in time (5 years) at the study area from 1.7 to 49.5 cm. They also found that the mean percentage cover of woody species for each year after the wildfire was: 1.5%, the first year after fire, 33%, the second year and 72% the third year. Our results agree with the observations above. We observed a rapid increase in vegetation cover until the third year after fire. After the third year, the rate of increase slowed (see Fig. 7). Vega et al. (2010) observed a similar recovery pattern dependent on burn severity in a zone near our study area: vegetation affected by lower burn severity level (unaffected crowns) recovered more height than vegetation highly affected by the fire.

Ecosystems (vegetation, soil, etc.) are damaged to a higher degree by more intense, severe and/or frequent fires that retard their post-fire recovery (Díaz-Delgado et al., 2003; Polychronaki et al., 2014). Our study estimated the resilience time of vegetation cover as 7, 13 and 20 years for vegetation affected by low, moderate and high burn severity level, respectively. Future studies based on longer VRI time series should validate the predicted resilience time for the high burn severity level in this study area. In any case, our estimated resilience values are reasonable and similar to those obtained in previous studies. Without using remotely sensed data, Barbero et al. (1998) found a recovery time value of 15 years in high seeding tree communities of Mediterranean *P. pinaster*. In high seeding tree communities of Mediterranean *P. halepensis*, different authors (Broncano et al., 2005; Kazanis and Arianoutsou, 2004; Trabaud, 2002) suggest recovery times starting from 15 years. Local attributes like climate, terrain characteristics, or vegetation type influence vegetation cover recovery time (Baeza et al., 2007; Keeley, 2009).

The added value of our method can be deduced from the three pillars on which it is based. First, it used MESMA fraction images instead of widely used spectral indices to characterize vegetation. Consequently, vegetation cover was more accurately represented as we used all reflectance bands information (instead of just information from two spectral bands), the influence of background effect of soil was reduced, and accurate estimates of vegetation abundance were even achieved when vegetation cover was low (first years after forest fire). Second, the study was based on VRI, calculated following the unburned control plot approach. Thus, reducing the influence of phenologic changes and making easier the visualization of the vegetation regeneration curve, as the same reference is considered as origin. Finally, we based the study on time series, what enabled us to trend model them and make predictions to estimate resilience.

Table 4
Trend models of VRI evolution in time curve for the three burn severity levels.

VRI	Trend models	a_0	a_1	RMSE	MAPE	AIC	RUNS	RUNM	AUTO	MEAN	VAR
VRI_h	Constant mean	0.2650	–	0.2203	49.5197	− 2.8712	OK	OK	OK	OK	***
	Linear	0.5152	− 0.0357	0.1784	44.5314	− 3.1574	***	*	OK	OK	**
	Exponential	− 0.7871	− 0.1023	0.1767	27.6738	− 3.1766	*	OK	OK	OK	***
VRI_m	Constant mean	0.1509	–	0.2004	154.0590	− 3.0623	*	OK	OK	OK	***
	Linear	0.4046	− 0.0362	0.1484	115.8900	− 3.5083	**	*	OK	OK	*
	Exponential	− 0.8669	− 0.2165	0.1324	33.6610	− 3.7365	*	OK	OK	OK	***
VRI_l	Constant mean	0.0698	–	0.1289	–	− 3.9434	OK	**	OK	*	***
	Linear	0.2386	− 0.0241	0.0922	–	− 4.4591	OK	*	OK	OK	*

VRI: vegetation recovery index; VRI_h: vegetation recovery index for high burn severity level; VRI_m: vegetation recovery index for moderate burn severity level; VRI_l: vegetation recovery index for low burn severity level; a_i: coefficients of the regression models; RMSE: root mean squared error; MAPE: mean absolute percentage error; AIC: Akaike information criterion; RUNS: test for excessive runs up and down; RUNM: test for excessive runs above and below median; AUTO: Box-Pierce test for excessive autocorrelation; MEAN: test for difference in mean 1st half to 2nd half; VAR: test for difference in variance 1st half to 2nd half; OK: not significant ($p \geq 0.05$); *: marginally significant ($0.01 < p \leq 0.05$); **: significant ($0.001 < p \leq 0.01$); ***: highly significant ($p \leq 0.001$).

Thus, although we proposed a new vegetation recovery index based on Landsat MESMA fraction images and studied its time evolution in a Mediterranean *P. pinaster* ecosystem, we are convinced the proposed index could be applicable to other Mediterranean and non-Mediterranean ecosystems (preferably with low fire recurrence), as far as candidate endmembers are carefully defined. Future research should check it. Equally, futures studies should verify whether the method is also adequate for resprouter ecosystems.

6. Conclusion

We report the first study based on MESMA fractions time series that analyzes post-fire vegetation recovery. We demonstrated that remote sensing techniques contribute to monitoring the post-fire forest cover recovery and result in a better understanding of the temporal regeneration of burned vegetation in forest Mediterranean ecosystems.

We implemented a MESMA-based methodology for modeling post-fire vegetation recovery in a Mediterranean *P. pinaster* ecosystem from Landsat data that was proven in Spain. The MESMA shade normalized GV fraction was referenced to the unburned class and a vegetation recovery index (VRI) was proposed. For each burn severity level considered: low, moderate and high, the evolution in time from 1999 to 2011 of VRI was analyzed and an estimation of the vegetation cover resilience was provided. We found that 7, 13, and 20 years are need by the vegetation cover affected by low, moderate and high burn severity level respectively to recover its previous to fire state. The agreement of these resilience times with the resilience times provided by other authors in similar ecosystems shows that the proposed methodology adequately models post-fire vegetation cover recovery. It is, however, necessary to remember that a meticulous choice of endmembers representing all existing land covers is a fundamental requirement in the accuracy of the MESMA fraction images. In this study, we incorporated both reference and image endmembers to build the candidate spectral library, and the definitive set of endmembers was selected by three indices: CoB, EAR and MASA.

We conclude that MESMA fraction images may be capable of helping us to study post-fire vegetation cover recovery processes and to understand the influence of burn severity on them, which may be valuable for fire management policies. Though our study was based on Mediterranean *P. pinaster* ecosystem, it could be extended to other Mediterranean ecosystems. Equally, our study may sustain future research as it provides a new perspective to post-fire ecosystem monitoring from multispectral satellite imagery.

Acknowledgments

The research work was financially supported by the Spanish Ministry of Economy and Competitiveness, and the European Regional Development Fund (ERDF) in the frame of the GES-FIRE project "Multi-scale tools for the post-fire management of fire prone ecosystems in the context of global change" (AGL201348189-C2-1-R). The second author was supported as research visitor at VIPER Lab. (University of California, Santa Barbara) by a Spanish Education Ministry grant (Salvador de Madariaga program, code PRX14/00160). We thank the anonymous reviewers and the editor for their comments, which significantly improved the content of this article.

References

Abdul-Malak, D., Pausas, J.G., Pardo-Pascual, J.E., Ruiz, L.A., 2015. Recurrence and the dynamics of the enhanced vegetation index in a Mediterranean ecosystem. Int. J. Appl. Geosp. Res. 6, 18–35.

Adams, J.B., Sabol, D.E., Kapos, V., Filho, R.A., Roberts, D.A., Smith, M.O., Gillespie, A.R., 1995. Classification of multispectral images based on fractions of endmembers: Application to land cover change in the Brazilian Amazon. Remote Sens. Environ. 52, 137–154.

Baeza, M.J., Valdecantos, A., Alloza, J.A., Vallejo, V.R., 2007. Human disturbance and environmental factors as drivers of long-term post-fire regeneration patterns in Mediterranean forest. J. Veg. Sci. 18, 243–252.

Barbero, M., Loisel, R., Quezel, P., Richardson, D.M., Romane, F., 1998. Pines of the Mediterranean basin. In: Richardson, D.M. (Ed.), Ecology and biogeography of Pinus. Cambridge University Press, Cambridge, pp. 153–170.

Bastos, A., Gouveia, C.M., DaCamara, C.C., Trigo, R.M., 2011. Modelling post-fire vegetation recovery in Portugal. Biogeosciences 8, 3593–3607.

Boardman, J.W., 1990. Inversion of high spectral resolution data. In: Proceedings SPIE, 1298, imaging spectroscopy, terrestrial. Environment, 222–233, Apr. 16–19, 1990, Orlando, Florida, (USA). .

Bolton, D.K., Coops, N.C., Wulder, M.A., 2015. Characterizing residual structure and forest recovery following high-severity fire in the western boreal of Canada using Landsat time-series and airborne lidar data. Remote Sens. Environ. 163, 48–60.

Broncano, M.J., Retana, J., Rodrigo, A., 2005. Predicting the recovery of Pinus halepensis and Quercus ilex forests after a large wildfire in northeastern Spain. Plant Ecol. 180, 47–56.

Calvo, L., Santalla, S., Marcos, E., Valbuena, L., Tárrega, R., Luis, E., 2003. Regeneration after wildfire in communities dominated by Pinus pinaster, an obligate seeder, and others dominated by Quercus pyrenaica, a typical resprouter. For. Ecol. Manag. 184, 209–223.

Calvo, L., Santalla, S., Valbuena, L., Marcos, E., Tárrega, R., Luis-Calabuig, L., 2008. Post-fire natural regeneration of a Pinus pinaster forest in NW Spain. Plant Ecol. 197, 81–90.

Calvo, L., Torres, O., Valbuena, L., Luis-Calabuig, E., 2013. Recruiment and early growth of Pinus pinaster seedlings over five years after a wildfire in NW Spain. For. Syst. 22, 582–586.

Canty, M.J., Nielsen, A.A., 2008. Automatic radiometric normalization of multitemporal satellite imagery with the iteratively re-weighted MAD transformation. Remote Sens. Environ. 112, 1025–1036.

Chander, G., Markham, B.L., Helder, D.L., 2009. Summary of current radiometric calibration coefficients for Landsat MSS, TM, ETM +, and EO-1 ALI sensors. Remote Sens. Environ. 113, 893–903.

Chavez Jr., P.S., 1989. Radiometric calibration of Landsat thematic mapper multispectral images. Photogramm. Eng. Remote. Sens. 55, 1285–1294.

Chavez Jr., P.S., 1996. Image-based atmospheric corrections – Revisited and improved. Photogramm. Eng. Remote. Sens. 62, 1025–1036.

Chen, X., Vogelmann, J.E., Rollins, M., Ohlen, D., Key, C.H., Yang, L., Huang, C., Shi, H., 2011. Detecting post-fire burn severity and vegetation recovery using multitemporal remote sensing spectral indices and field-collected composite burn index data in a ponderosa pine forest. Int. J. Remote Sens. 32, 7905–7927.

Chen, W., Moriya, K., Sakai, T., Koyama, L., Cao, C., 2014. Monitoring of post-fire forest recovery under different restoration modes based on time series Landsat data. Eur. J. Remote Sens. 47, 153–168.

Chu, T., Guo, X., 2014. Remote sensing techniques in monitoring post-fire effects and patterns of forest recovery in boreal forest regions: A review. Remote Sens. 6, 470–520.

Chuvieco, E. (Ed.), 2009. Earth observation of wildland fires in Mediterranean ecosystems. Springer, Heidelberg Dordrecht London New York.

Covington, W.W., Sackett, S.S., 1992. Soil mineral nitrogen changes following prescribed burning in ponderosa pine. For. Ecol. Manag. 54, 175–191.

Dennison, P.E., Roberts, D.A., 2003. Endmember selection for multiple endmember spectral mixture analysis using endmember average RMSE. Remote Sens. Environ. 87, , 123–135.

Dennison, P.E., Roberts, D.A., 2003. The effects of vegetation phenology on endmember selection and species mapping in Southern California chaparral. Remote Sens. Environ. 87, , 295–309.

Dennison, P.E., Halligan, K.Q., Roberts, D.A., 2004. A comparison of error metrics and constraints for multiple endmember spectral mixture analysis and spectral angle mapper. Remote Sens. Environ. 93, 359–367.

Di Mauro, B., Fava, F., Busetto, L., Crosta, G.F., Colombo, R., 2014. Post-fire resilience in the Alpine region estimated from MODIS satellite multispectral data. Int. J. Appl. Earth Obs. Geoinf. 32, 163–172.

Díaz-Delgado, R., Pons, X., 2001. Spatial patterns of forest fires in Catalonia (NE of Spain) along the period 1975–1995. Analysis of vegetation recovery after fire. For. Ecol. Manag. 147, 67–74.

Díaz-Delgado, R., Lloret, F., Pons, X., Terradas, J., 2002. Satellite evidence of decreasing resilience in Mediterranean plant communities after recurrent wildfires. Ecology 83, 2293–2303.

Díaz-Delgado, R., Lloret, F., Pons, X., 2003. Influence of fire severity on plant regeneration by means of remote sensing imagery. Int. J. Remote Sens. 24, 1751–1763.

Dubovyk, O., Landmann, T., Erasmus, B.F.N., Tewes, A., Schellberg, J., 2015. Monitoring vegetation dynamics with medium resolution MODIS-EVI time series at sub-regional scale in southern Africa. Int. J. Appl. Earth Obs. Geoinf. 38, 175–183.

Dudley, K.L., Dennison, P.E., Roth, K.L., Roberts, D.A., Coates, A.R., 2015. A multi-temporal spectral library approach for mapping vegetation species across spatial and temporal phenological gradients. Remote Sens. Environ. 167, 121–134.
Elmore, A., Mustard, J., Manning, S., Lobell, D., 2000. Quantifying vegetation change in semiarid environments: Precision and accuracy of spectral mixture analysis and the normalized difference vegetation index. Remote Sens. Environ. 73, 87–102.
Fernández-Manso, O., Quintano, C., Fernández-Manso, A., 2009. Combining spectral mixture analysis and object-based classification for fire severity mapping. For. Syst. 18, 296–313.
Gitas, I., Mitri, G., Veraverbeke, S., Polychronaki, A., 2012. Advances in remote sensing of post-fire vegetation recovery monitoring – A review. In: Fatoyinbo, L. (Ed.), 'Remote sensing of biomass – principles and applications'. InTech.
Goetz, S.J., Fiske, G.J., Bunn, A.G., 2006. Using satellite time-series data sets to analyze fire disturbance and forest recovery across Canada. Remote Sens. Environ. 101, 352–365.
He, C., Wei, A., Shi, P., Zhang, Q., Zhao, Y., 2011. Detecting land-use/land-cover change in rural-urban fringe areas using extended change-vector analysis. Int. J. Appl. Earth Obs. Geoinf. 13, 572–585.
Herold, M., Roberts, D.A., Gardner, M.E., Dennison, P.E., 2004. Spectrometry for urban area remote sensing — Development and analysis of a spectral library from 350 to 2400 nm. Remote Sens. Environ. 91, 304–319.
Herranz, J.M., Martínez-Sánchez, J.J., Marín, A., Ferrandis, P., 1997. Post-fire regeneration of Pinus halepensis Miller in a semi-arid area in Albacete province (southeastern Spain). Ecoscience 4, 86–90.
Herrero, C., San Martin, R., Bravo, F., 2007. Effect of heat and ash treatments on germination of Pinus pinaster and Cistus laurifolius. J. Arid Environ. 70, 540–548 (2007).
Hostert, P., Röder, A., Hill, J., 2003. Coupling spectral unmixing and trend analysis for monitoring of long-term vegetation dynamics in Mediterranean rangelands. Remote Sens. Environ. 87, 183–197.
Idris, M., Kuraji, K., Suzuki, M., 2005. Evaluating vegetation recovery following large-scale forest fires in Borneo and northeastern China using multi-temporal NOAA/AVHRR images. J. For. Res. 10, 101–111.
Ireland, G., Petropoulos, G.P., 2015. Exploring the relationships between post-fire vegetation regeneration dynamics, topography and burn severity: A case study from the Montane Cordillera Ecozones of Western Canada. Appl. Geogr. 56, 232–248.
Jakubauskas, M.E., Lulla, K.P., Mausel, P.W., 1990. Assessment of vegetation change in a fire-altered forest landscape. Photogramm. Eng. Remote. Sens. 56, 371–377.
Kaufman, Y.J., 1989. The atmospheric effect on remote sensing and its corrections. In: Asrar, G. (Ed.), Theory and Applications of Optical Remote Sensing. Wiley-Interscience, New York, NY, pp. 336–428.
Kazanis, D., Arianoutsou, M., 2004. Long-term post-fire vegetation dynamics in Pinus halepensis forests of Central Greece: A functional group approach. Plant Ecol. 171, 101–121.
Keeley, J.E., 1986. Resilience of Mediterranean shrub communities to fire. In: Dell, B., Hopkins, A.J.M., Lamont, B.B. (Eds.), Resilience in Mediterranean-type ecosystems. Dr. W. Junk Publishers, Dordrecht, pp. 95–112 (168 pp)..
Keeley, J.E., 2009. Fire intensity, fire severity and burn severity: A brief review and suggested usage. Int. J. Wildland Fire 18, 116–126.
Keeley, J.E., Bond, W.J., Bradstock, R.A., Pausas, J.G., Rundel, P.W., 2012. Fire in mediterranean ecosystems: Ecology, evolution and management. Cambridge University Press.
Key, C.H., Benson, N.C., 2006. Landscape assessment: Ground measure of severity, the composite burn index; and remote sensing of severity, the normalized burn ratio. In: Lutes, D.C., Keane, R.E., Caratti, J.F., Key, C.H., Benson, N.C., Sutherland, S., Gangi, L.J. (Eds.), FIREMON: Fire effects monitoring and inventory system. USDA forest service, Rocky Mountain Research Station, Ogden, UT. Gen. Tech. Rep. RMRS-GTR-164-CD: LA pp. 1–51.
Lanorte, A., Lasaponara, R., Lovallo, M., Telesca, L., 2014. Fisher–Shannon information plane analysis of SPOT/VEGETATION normalized difference vegetation index (NDVI) time series to characterize vegetation recovery after fire disturbance. Int. J. Appl. Earth Obs. Geoinf. 26, 441–446.
Lee, S.W., Lee, M.B., Lee, Y.G., Won, M.S., Kim, J.J., Hong, S., 2009. Relationship between landscape structure and burn severity at the landscape and class levels in Samchuck, South Korea. For. Ecol. Manag. 258, 1594–1604.
Lhermitte, S., Verbesselt, J., Verstraeten, W.W., Coppin, P., 2010. A pixel based regeneration index using time series similarity and spatial context. Photogramm. Eng. Remote. Sens. 76, 673–682.
Lhermitte, S., Verbesselt, J., Verstraeten, W.W., Veraverbeke, S., Coppin, P., 2011. Assessing intra-annual vegetation regrowth after fire using the pixel based regeneration index. ISPRS J. Photogramm. Remote Sens. 66, 17–27.
Li, L., Ustin, S.L., Lay, M., 2005. Application of multiple endmember spectral mixture analysis (MESMA) to AVIRIS imagery for coastal salt marsh mapping: A case study in China camp, CA, USA. Int. J. Remote Sens. 26, 5193–5207.
Li, M., Qu, J., Hao, X., 2008. Detecting vegetation change with satellite remote sensing over 2007 Georgia wildfire regions. J. Appl. Remote. Sens. 2, 021505.
Maia, P., Juli, G., Pausas, J., Vasques, A., Keizer, J.J., 2012. Fire severity as a key factor in post-fire regeneration of Pinus pinaster (Ait.) in Central Portugal. Ann. For. Sci. 69, 489–498.
Maselli, F., 1998. Multiclass spectral decomposition of remotely sensed scenes by selective pixel unmixing. IEEE Trans. Geosci. Remote Sens. 36, 1809–1820.
Meng, R., Dennison, P.E., Huang, C., Moritz, M.A., D'Antonio, C., 2015. Effects of fire severity and post-fire climate on short-term vegetation recovery of mixed-conifer and red fir forests in the Sierra Nevada Mountains of California. Remote Sens. Environ. 171, 311–325.
Moreira, F., Viedma, O., Arianoutsou, M., Curt, T., Koutsias, N., Rigolot, E., Barbati, A., Corona, P., Vaz, P., Xanthopoulos, G., Mouillot, F., Bilgili, E., 2011. Landscape – Wildfire interactions in Southern Europe: Implications for landscape management. J. Environ. Manag. 92, 2389–2402.
Neary, D.G., Klopatek, C.C., DeBano, L.F., Ffolliott, P.F., 1999. Fire effects on belowground sustainability: A review and synthesis. For. Ecol. Manag. 122, 51–71.
Okin, G.S., Okin, W.J., Murray, B., Roberts, D.A., 2001. Practical limits on hyperspectral vegetation discrimination in arid and semiarid environments. Remote Sens. Environ. 77, 212–225.
Patterson, M.W., Yool, S.R., 1998. Mapping fireinduced vegetation mortality using Landsat thematic mapper data: A comparison of linear transformation techniques. Remote Sens. Environ. 65, 132–142.
Pausas, J.G., Llovet, J., Rodrigo, A., Vallejo, R., 2008. Are wildfires a disaster in the Mediterranean basin? – A review. Int. J. Wildland Fire 17, 713–723.
Petropoulos, G.P., Griffiths, H.M., Kalivas, D.P., 2014. Quantifying spatial and temporal vegetation recovery dynamics following a wildfire event in a Mediterranean landscape using EO data and GIS. Appl. Geogr. 50, 120–131.
Polychronaki, A., Gitas, I.Z., Minchella, A., 2014. Monitoring post-fire vegetation recovery in the Mediterranean using SPOT and ERS imagery. Int. J. Wildland Fire 23, 631–642.
Powell, R.L., Roberts, D.A., Dennison, P.E., Hess, L.L., 2007. Sub-pixel mapping of urban land cover using multiple endmember spectral mixture analysis: Manaus, Brazil. Remote Sens. Environ. 106, 253–267.
Quintano, C., Fernández-Manso, A., Shimabukuro, Y.E., Pereira, G., 2012. Spectral unmixing: A review. Int. J. Remote Sens. 33, 5307–5340.
Quintano, C., Fernández-Manso, A., Roberts, D.A., 2013. Multiple endmember spectral mixture analysis (MESMA) to map burn severity levels from Landsat images in Mediterranean countries. Remote Sens. Environ. 136, 76–88.
Riaño, D., Chuvieco, E., Ustin, S., Zomer, R., Dennison, P., Roberts, D., Salas, J., 2002. Assessment of vegetation regeneration after fire through multitemporal analysis of AVIRIS images in the Santa Monica Mountains. Remote Sens. Environ. 79, 60–71.
Roberts, D.A., Gardner, M., Church, R., Ustin, S.L., Scheer, G., Green, R.O., 1998. Mapping chaparral in the Santa Monica Mountains using multiple endmember spectral mixture models. Remote Sens. Environ. 65, 267–279.
Roberts, D.A., Dennison, P.E., Gardner, M., Hetzel, Y., Ustin, S.L., Lee, C., 2003. Evaluation of the potential of hyperion for fire danger assessment by comparison to the airborne visible/infrared imaging spectrometer. IEEE Trans. Geosci. Remote Sens. 41, 1297–1310.
Roberts, D.A., Halligan, K., Dennison, P., 2007. VIPER Tools User Manual. V1.5. .
Roberts, D.A., Quattrochi, D.A., Hulley, G.C., Hook, S.J., Green, R.O., 2012. Synergies between VSWIR and TIR data for the urban environment: An evaluation of the potential for the hyperspectral infrared imager (HyspIRI) decadal survey mission. Remote Sens. Environ. 117, 83–101.
Röder, A., Hill, J., Duguy, B., Alloza, J.A., Vallejo, R., 2008. Using long time series of Landsat data to monitor fire events and post-fire dynamics and identify driving factors. A case study in the Ayora region (eastern Spain). Remote Sens. Environ. 112, 259–273.
Rodrigues, M., Ibarra, P., Echeverría, M., Pérez-Cabello, F., de la Riva, J., 2014. A method for regional-scale assessment of vegetation recovery time after high-severity wildfires: Case study of Spain. Prog. Phys. Geogr. 38, 556–575.
Rogan, J., Franklin, J., 2001. Mapping wildfire burn severity in Southern California forests and shrublands using enhanced thematic mapper imagery. Geocarto Int. 16, 91–101.
Rogan, J., Yool, S.R., 2001. Mapping fire-induced vegetation depletion in the Peloncillo Mountains, Arizona and New Mexico. Int. J. Remote Sens. 22 (16), 3101–3121.
Román, M.A., Azqueta, D., Rodrigues, M., 2013. Methodological approach to assess the socio-economic vulnerability to wildfires in Spain. For. Ecol. Manag. 294, 158–165.
Ruíz-Gallardo, J.R., Castaño, S., Calera, A., 2004. Application of remote sensing and GIS to locate priority intervention areas after wildland fires in Mediterranean systems: A case study from southeastern Spain. Int. J. Wildland Fire 13, 241–252.
Sankey, T., Moffet, C., Weber, K., 2008. Postfire recovery of sagebrush communities: Assessment using SPOT-5 and very large-scale aerial imagery. Rangel. Ecol. Manag. 61, 598–604.

Sá-Torres, J.P.C., 2013. Patterns and drivers of wildfire occurrence and post-fire vegetation resilience across scales in Portugal (Dissertation PhD) University of Porto (Portugal).
Sever, L., Leach, J., Bren, L., 2012. Remote sensing of post-fire vegetation recovery; a study using Landsat 5 TM imagery and NDVI in North-East Victoria. J. Spat. Sci. 57, 75–191.
Shimabukuro, Y.E., Smith, J.A., 1991. The least-squares mixing models to generate fraction images derived from remote sensing multispectral data. IEEE Trans. Geosci. Remote Sens. 29, 16–20.
Silva, J.S.,.P., Vaz, F., Moreira, F., Catry, Rego, F.C., 2011. Wildfires as a major driver of landscape dynamics in three fire-prone areas of Portugal. Landsc. Urban Plan. 101, 349–358.
Silván-Cárdenas, J.L., Wang, L., 2014. On quantifying post-classification subpixel landcover changes. ISPRS J. Photogramm. Remote Sens. 98, 94–105.
Smith, A.M., Lentile, L.B., Hudak, A.T., Morgan, P., 2007. Evaluation of linear spectral unmixing and DNBR for predicting post-fire recovery in a North American ponderosa pine forest. Int. J. Remote Sens. 28, 5159–5166.
Smithwick, E.A.H., Turner, M.G., Mack, M.C., Chapin, F.S., 2005. Postfire soil N cycling in northern conifer forests affected by severe, stand-replacing wildfires. Ecosystems 8, 163–181.
Song, C., Woodcock, C.E., Seto, K.C., Lenney, M.P., Macomber, A.S., 2001. Classification and change detection using Landsat TM data: When and how to correct atmospheric effects. Remote Sens. Environ. 75, 230–244.
Souza Jr., C., Firestone, L., Silva, L.M., Roberts, D., 2003. Mapping forest degradation in the eastern Amazon from SPOT 4 through spectral mixture models. Remote Sens. Environ. 87, 494–506.
Tapias, R., Climent, J., Pardos, J.A., Gil, L., 2004. Life histories of Mediterranean pines. Plant Ecol. 171, 53–68.
Technologies, S., 2012. Manual statgraphics centurion XVI. Statpoint technologies (Ed.). .
Teillet, P.M., Guindon, B., Goodenough, D.G., 1982. On the slope-aspect correction of multispectral scanner data. Can. J. Remote Sens./J. Can. Télédét. 8, 84–106.
Thanos, C.A., Daskakakou, E.N., Nikolaidou, S., 1996. Early post-fire regeneration of a Pinus halepensis forest on Mount Parnis, Greece. J. Veg. Sci. 7, 273–280.
Tompkins, S., Mustard, J.F., Pieters, C.M., Forsyth, D.W., 1997. Optimization of endmembers for spectral mixture analysis. Remote Sens. Environ. 59, 472–489.
Trabaud, L., 2002. Post-fire vegetation recovery and dynamics in the Mediterranean area. In: Pardini, G., Pintó, J. (Eds.), Fire, landscape and biodiversity: An appraisal of the effects and effectiveness. Lectures from the 3rd international summer school on the environment. Universitat de Girona, Institut de Medi Ambient, Girona, pp. 39–56.
Twele, A., 2004. Post-fire vegetation regeneration. In: The case study of the Masif de l'Étoile fire. European commission, directorate general joint research centre (EUR 21010). .
van der Meer, F.D., Jia, X., 2012. Collinearity and orthogonality of endmembers in linear spectral unmixing. Int. J. Appl. Earth Obs. Geoinf. 18, 491–503.
van Leeuwen, W.J.D., Casady, G.M., Neary, D.G., Bautista, S., Alloza, J.A., Carmel, Y., Wittenberg, L., Malkinson, D., Orr, B.J., 2010. Monitoring post-wildfire vegetation response with remotely sensed time-series data in Spain, USA and Israel. Int. J. Wildland Fire 19, 75–93.
Vega, J.A., Fernández, C., Pérez-Gorostiaga, P., Fonturbe, T., 2010. Response of maritime pine (Pinus pinaster Ait.) recruitment to fire severity and post-fire management in a coastal burned area in Galicia (NW Spain). Plant Ecol. 206, 297–308.
Veraverbeke, S., Lhermitte, S., Verstraeten, W.W., Goossens, R., 2011. A time integrated MODIS burn severity assessment using the multi-temporal differenced normalized burn ratio (dNBRMT). Int. J. Appl. Earth Obs. Geoinf. 13, 52–58.
Veraverbeke, S., Somers, B., Gitas, I., Katagis, T., Polychronaki, A., Goossens, R., 2012. Spectral mixture analysis to assess post-fire vegetation regeneration using Landsat thematic mapper imagery: accounting for soil brightness variation. Int. J. Appl. Earth Obs. Geoinf. 14, 1–11.
Vicente-Serrano, S.M., Pérez-Cabello, F., Lasanta, T., 2011. Pinus halepensis regeneration after a wildfire in a semiarid environment: Assessment using multitemporal Landsat images. Int. J. Wildland Fire 20, 195–208.
Vila, G., Barbosa, P., 2010. Post-fire vegetation regrowth detection in the Deiva Marina region (Liguria-Italy) using Landsat TM and ETM + data. Ecol. Model. 221, 75–84.
White, D., Minotti, P., Barczak, M., Sifneos, J., Freemark, K., Santelmann, M., Steinitz, C., Ross, Kiester, A., Preston, C., 1997. Assessing risks to biodiversity from future landscape change. Conserv. Biol. 11, 349–360.
Yang, X., Lo, C.P., 2000. Relative radiometric normalization for change detection from multi-date satellite images. Photogramm. Eng. Remote. Sens. 66, 967–980.